Effects of Spacer Chain Lengths on Layered Nanostructures Assembled with Main-Chain Azobenzene Ionenes and Polyelectrolytes

Jong-Dal Hong* and Byung-Duk Jung

Department of Chemistry, University of Inchon, 177 Dohwa-dong Nam-ku, Inchon 402-749, S. Korea

Chang Hwan Kim and Kwan Kim

Division of Chemistry and Molecular Engineering and Center for Molecular Catalysis, Seoul National University, Seoul 151-742, S. Korea

Received February 17, 2000

ABSTRACT: With the aim of fabricating internally ordered multilayer assemblies using the layer-by-layer electrostatic deposition method, we have prepared polyelectrolytes called ionenes that contain rigid azobenzene chromophores separated by flexible spacer chains, i.e., poly(((4,4′-bis(6-dimethylammonio)-hexyl)oxy)azobenzene bromide), PAZ-6, poly(((4,4′-bis(10-dimethylammonio)decyl)oxy)azobenzene bromide), PAZ-10, and poly(((4,4′-bis(12-dimethylammonio)dodecyl)oxy)azobenzene bromide), PAZ-12. UV/vis spectroscopy of solutions shows that PAZ-10 and PAZ-12 form robust lamellar aggregates that could be successfully transferred onto a solid substrate by forming multilayer assemblies with oppositely charged polyelectrolytes. From FTIR spectra of the resulting multilayer assemblies, the alkyl chains appeared to be highly ordered, especially in the case of longer spacer chain. The thicknesses of the PAZ monolayers measured atomic force microscopy were overall consistent with the theoretical values (2.61 and 3.23 nm) determined by a model calculation, based on the tilt angle measurement of chromophore and the molecular length of the repeat unit of the ionenes.

1. Introduction

During recent years, the layer-by-layer self-assembly technique based on electrostatic attraction between opposite charges[1] has been used for the nanofabrication of a wide variety of heterostructures on a solid substrate. From basic assembly of cationic and anionic polyelectrolytes,[2] the method has been extended to polyelectrolytes and DNA,[3] polyelectrolytes and latex particles,[4] polyelectrolytes and proteins,[5] polyelectrolytes and delaminated clay platelets,[6−9] polyelectrolytes and colloidal metal particles,[10−12] polyelectrolytes and dyes,[13−18] and polyelectrolytes and electrically conductive or electroluminescent conjugated polymers.[19,20]

Despite the variety of these multilayer assemblies, the resulting heterostructures do not normally show the marked multilayer ordering which might be expected from the layer-by-layer fabrication procedure. Mallouk and co-workers have attempted to enhance the electron density contrast of electrostatic self-assembly and hinder the interpenetration of the anionic layers into the adjacent cationic layers. The blocking layers can be inorganic, e.g. semiinfinite, two-dimensional inorganic sheets of α-zirconium phosphate.[21] To achieve an internal ordering in layers, they can also be organic, by choosing one of the polyelectrolyte layers with liquid crystalline[22] or amphiphilic[1,23−27] properties.

Using the organic approach, order in the direction perpendicular to the surface has been demonstrated under appropriate adsorption conditions.[27] Now, we extend these concepts to prepare ordered multilayers by using ionenes that are built up with a bipolar amphiphile as a repeat unit. Kunitake and co-workers[28] have also shown that oligomeric ammonium amphiphiles, which they call ionenes, form a monolayer membrane in aqueous solution when the spacer length is at least C_{10}, as shown in Figure 1.

The aim of the present work is to improve the internal order of these layer-by-layer electrostatically adsorbed films. We have therefore prepared cationic polyelectrolytes similar to the ionenes of Kunitake et al. As shown in Scheme 1, they contain a rigid symmetrical azobenzene chromophore separated by flexible spacer chains of 6, 10, and 12 methylenes in length. The present study reports the formation of multilayer assemblies by deposition onto the substrate alternately of ionene membranes self-assembled in solution and of anionic polyelectrolyte. An idealized schematic view is shown in Figure 1. In addition, we report the dependence of the morphology of the multilayer assemblies on the spacer chain length of the ionenes studied using polarized UV/vis and FTIR spectroscopy, ellipsometry, and atomic force microscopy (AFM).

2. Experimental Section

2.1. Materials. Poly(allylamine hydrochloride) (M_n = 50 000−65 000), PAH, and ι-carrageenan, CAG, were purchased from Aldrich and used without further purification.

2.2. Synthesis of Ionenes. The ionenes with the spacer chain length with 6, 10, and 12 carbons, i.e., poly(((4,4′-bis(6-dimethylammonio)hexyl)oxy)azobenzene bromide), poly(((4,4′-bis(10-dimethylammonio)decyl)oxy)azobenzene bromide), and poly(((4,4′-bis(12-dimethylammonio)dodecyl)oxy)azobenzene bromide), were synthesized in four steps in similar manner based on the modified literature processes,[28,29] and the molecular structures are given in Scheme 1. The synthetic route for the polyion PAZ-12 is described here as an example. First, a reductive coupling of *p*-nitrophenol with KOH leads to the 4,4′-dihydroxyazobenzene. Second, the 4,4′-dihydroxyazobenzene was converted to 4,4′-bis((12-bromododecyl)oxy)azobenzene by Williamson's ether synthesis with 1,12-dibromododecane. Third, the 4,4′-bis((12-(dimethylamino)dodecyl)oxy)azobenzene was

* To whom all correspondence should be addressed. Tel 82-32-770-8234, FAX 82-32-770-8238, e-mail hong5506@lion.inchon.ac.kr or hong5506@hanmail.net (alternative).

10.1021/ma000293g CCC: $19.00
Published on Web 10/17/2000

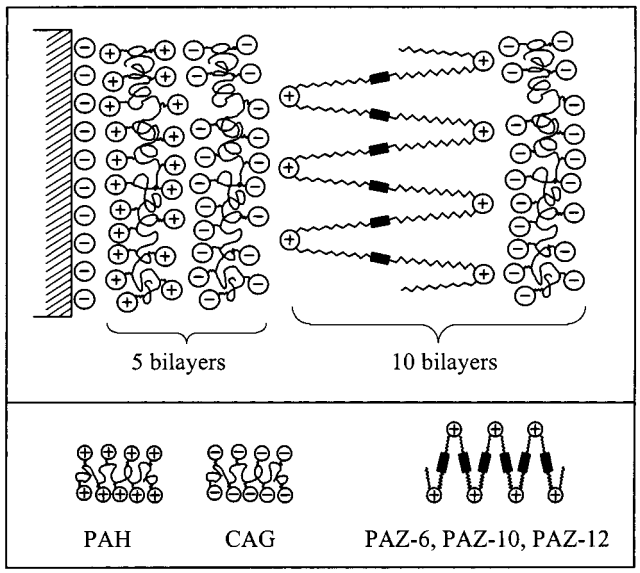

Figure 1. An idealized schematic view of an alternating multilayer assemblies of cationic ionenes PAZ and an anionic polyelectrolyte *ι*-carrageenan (CAG).

Scheme 1

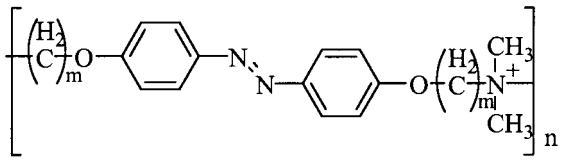

PAZ-6 (m=6), PAZ-10 (m=10), PAZ-12 (m=12)

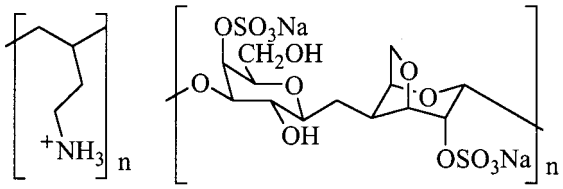

PAH CAG

obtained by the reaction of dimethylamine and 4,4′-bis((12-bromododecyl)oxy)azobenzene in toluene. Finally, the PAZ-12 was prepared by the addition polymerization of the corresponding diamine and dibromide: 4,4′-bis((12-bromododecyl)-oxy)azobenzene and 4,4′-bis((12-(dimethylamino)dodecyl)oxy)-azobenzene. The synthesis of 4,4′-dihydroxyazobenzene and 4,4′-bis((12-bromododecyl)oxy)azobenzene has been already described in the published literature.[27] 4,4′-Bis((6-bromohexyl)-oxy)azobenzene and 4,4′-bis((10-bromodecyl)oxy)azobenzene were also synthesized in a similar manner.

4,4′-Bis((12-(dimethylammonio)dodecyl)oxy)azobenzene. 4,4′-Bis((12-bromododecyl) oxy)azobenzene (1.64 g, 2.3 mmol) was dissolved in toluene and allowed to react with a large excess of dimethylamine in a sealed ampule at 100 °C for 125 h. The precipitate was removed, and after evaporation of the solvent, the crude residue was dissolved in $CHCl_3$/MeOH (2/1) and purified via column chromatography (Silicagel, Aldrich 70−230 mesh). Yield: 52%. Melting point: 89 °C. ^{1}H NMR ($CDCl_3$, 200 MHz, ppm): δ 1.21 (m, $-CH_2(CH_2)_8CH_2-$, 32H), δ 1.36 (m, $-CH_2CH_2N(CH_3)_2-$, 4H), δ 1.74 (m, $-CH_2CH_2-(CH_2)_8-$, 4H), δ 2.15 (m, $-CH_2N(CH_3)_2$, 16H), δ 3.98 (t, $-O-CH_2CH_2-$, 4H), δ 6.94 (d, phenyl ring, $4H_a$), δ 7.81 (d, phenyl ring, $4H_b$). IR (FT-IR, KBr, cm^{-1}): 2925 (CH_2, ν_{as}), 2845 (CH_2, ν_s), 1600 (benzene, ν_{as}), 1245 (Ph−O−C, ν_{as}), 1151 (C−N, ν_s). Anal. Calcd: C, 75.42; H, 10.76; N, 8.79. Found: C, 74.97; H, 10.60; N, 8.95.

4,4′-Bis((10-(dimethylammonio)decyl)oxy)azobenzene. 4,4′-Bis((10-bromodecyl)oxy)azobenzene was similarly converted to the dimethylamino derivative by reaction at 100 °C for 157 h. The crude residue was dissolved in $CHCl_3$/MeOH (2/1) and purified via column chromatography (Silicagel, Aldrich 70−230 mesh). Yield: 90%. Melting point: 100 °C. ^{1}H NMR ($CDCl_3$, 200 MHz, ppm): δ 1.28 (m, $-CH_2(CH_2)_7CH_2-$, 28H), δ 1.80 (m, $-CH_2CH_2(CH_2)_8-$, 4H), δ 2.18 (m, $-CH_2N(CH_3)_2$, 16H), δ 4.01 (t, $-O-CH_2CH_2-$, 4H), δ 6.98 (d, phenyl ring, $4H_a$), δ 7.85 (d, phenyl ring, $4H_b$). IR (FT-IR, KBr, cm^{-1}): 2926 (CH_2, ν_{as}), 2849 (CH_2, ν_s), 1602 (benzene, ν_{as}), 1245 (Ph−O−C, ν_{as}), 1148 (C−N, ν_s). Anal. Calcd: C, 74.44; H, 10.41; N, 9.64. Found: C, 74.59; H, 9.79; N, 8.78.

4,4′-Bis((6-(dimethylammonio)hexyl)oxy)azobenzene. 4,4′-Bis((6-bromohexyl)oxy)azobenzene was similarly converted to the dimethylamino derivative by reaction at 100 °C for 137 h. The crude residue was dissolved in $CHCl_3$/MeOH (2/1) and purified via column chromatography (Silicagel, Aldrich 70−230 mesh). Yield: 69%. Melting point: 92 °C. ^{1}H NMR ($CDCl_3$, 200 MHz, ppm): δ 1.48 (m, $-CH_2(CH_2)_3CH_2-$, 12H), δ 1.80 (q, $-OCH_2CH_2(CH_2)_4-$, 4H), δ 2.27 (m, $-CH_2N(CH_3)_2$, 16H), δ 4.03 (t, $-O-CH_2CH_2-$, 4H), δ 6.97 (d, phenyl ring, $4H_a$), δ 7.86 (d, phenyl ring, $4H_b$). IR (FT-IR, KBr, cm^{-1}): 2930 (CH_2, ν_{as}), 2858 (CH_2, ν_s), 1602 (benzene, ν_{as}), 1245 (Ph−O−C, ν_{as}), 1148 (C−N, ν_s). Anal. Calcd: C, 71.76; H, 9.46; N, 11.95. Found: C, 71.82; H, 9.39; N, 11.78.

Poly(((4,4′-bis(12-dimethylammonio)dodecyl)oxy)azobenzene bromide). 4,4′-Bis(12-bromododecyloxy)azobenzene (0.89 g, 1.3 mM) and 4,4′-bis(12-dimethylaminododecyloxy)-azobenzene (0.83 g, 1.3 mM) in 30 mL of THF was stirred at 80 °C for 252 h. The product precipitated. The row product dissolved in warm DMSO was added dropwise to THF with magnetic stirring. The polymer was isolated by filtration. Yield: 37%. Melting point: 148 °C. ^{1}H NMR (DMSO-d_6, 500 MHz): δ 1.25 (m, $-CH_2(CH_2)_9CH_2-$, 12H), δ 1.70 (m, $-OCH_2CH_2(CH_2)_{10}-$, 4H), δ 2.95 (m, $-CH_2N^+(CH_3)_2CH_2-$, 4H), δ 3.00 (s, $-CH_2N^+(CH_3)_2CH_2-$, 6H), δ 4.02 (t, $-O-CH_2-CH_2-$, 4H), δ 7.08 (d, phenyl ring, $4H_a$), δ 7.81 (d, phenyl ring, $4H_b$). IR (FT-IR, KBr, cm^{-1}): 2925 (CH_2, ν_{as}), 2853 (CH_2, ν_s), 1601 (benzene, ν_{as}), 1246 (Ph−O−C, ν_{as}), 1148 (C−N, ν_s), 1030 (Ph−O−C, ν_s). Anal. Calcd: C, 67.83; H, 9.29; N, 6.24. Found: C, 68.53; H, 9.12; N, 6.43.

Poly(((4,4′-bis(10-dimethylammonio)decyl)oxy)azobenzene bromide). Poly(((4,4′-bis(10-dimethylammonio)decyl)-oxy)azobenzene bromide) was also synthesized in a similar manner like poly(((4,4′-bis(12-dimethylammonio)dodecyl)oxy)-azobenzene bromide). Yield: 52%. Melting point: 203−210 °C. ^{1}H NMR (DMSO-d_6, 500 MHz): δ 1.26 (m, $-CH_2(CH_2)_7CH_2-$, 28H), δ 1.67 (m, $-CH_2CH_2(CH_2)_8-$, 4H), δ 3.00 (m, $-CH_2N^+(CH_3)_2CH_2-$, 10H), δ 3.97 (t, $-O-CH_2CH_2-$, 4H), δ 6.98 (d, phenyl ring, $4H_a$), δ 7.75 (d, phenyl ring, $4H_b$). IR (FT-IR, KBr, cm^{-1}): 2928 (CH_2, ν_{as}), 2854 (CH_2, ν_s), 1596 (benzene, ν_{as}), 1250 (Ph−O−C, ν_{as}), 1151 (C−N, ν_s), 1030 (Ph−O−C, ν_s). Anal. Calcd: C, 66.21; H, 8.83; N, 6.81. Found: C, 65.97; H, 8.78; N, 6.55.

Poly(((4,4′-bis(6-dimethylammonio)hexyl)oxy)azobenzene bromide). Poly(((4,4′-bis(6-dimethylammonio)hexyl)-oxy)azobenzene bromide) was synthesized in a similar manner like poly(((4,4′-bis(12-dimethylammonio)dodecyl)oxy)azobenzene bromide). Yield: 64%. Melting point: 220−230 °C. ^{1}H NMR (DMSO-d_6, 500 MHz): δ 1.36 (m, $-CH_2(CH_2)_3CH_2-$, 12H), δ 1.71 (m, $-OCH_2CH_2(CH_2)_4-$, 4H), δ 2.95 (m, $-CH_2N^+(CH_3)_2CH_2-$, 4H), δ 3.00 (s, $-CH_2N^+(CH_3)_2CH_2-$, 6H), δ 4.03 (t, $-O-CH_2CH_2-$, 4H), δ 7.06 (d, phenyl ring, $4H_a$), δ 7.79 (d, phenyl ring, $4H_b$). IR (FT-IR, KBr, cm^{-1}): 2939 (CH_2, ν_{as}), 2862 (CH_2, ν_s), 1596 (benzene, ν_{as}), 1250 (Ph−O−C, ν_{as}), 1149 (C−N, ν_s), 1030 (Ph−O−C, ν_s). Anal. Calcd: C, 61.89; H, 7.59; N, 8.33. Found: C, 60.94; H, 7.56; N, 8.12.

The polymerization conditions for the PAZ-6, PAZ-10, and PAZ-12 are summarized in Table 1.

2.3. Multilayer Preparation. The ultrapure water used for all experiments and all cleaning steps was obtained by an ion-exchange and filtration unit (Milli-Q, Millipore GmbH). The resistivity was better than 18.0 MΩ·cm. The substrates for all adsorption experiments were fused silica slides of size

Table 1. Polymerization Conditions for the Ionenes PAZ-6, PAZ-10, and PAZ-12

ionenes	total monomer concn (M)	solvent	temp (°C)	time (h)	yield (%)	DP[a] (X_n)
PAZ-12	0.087	THF	80	252	37	13−14
PAZ-10	0.034	THF	60	336	52	16−17
PAZ-6	0.025	THF	60	237	64	15−16

[a] The degree of polymerization (X_n) was calculated based on the integral of the characteristic NMR signals of a dimethylamino end group and a dimethyl group linked to the ammonium nitrogen which could be determined from the 500 MHz ^{1}H NMR spectra of the PAZ-6, PAZ-10, and PAZ-12.

25 × 50 mm^2. They were cleaned by ultrasonication in the mixture of H_2SO_4/H_2O_2 (7/3) and then heated in the mixture of $H_2O/H_2O_2/NH_3$ (5:1:1) at 80 °C for 1 h. The substrates were thoroughly washed with ultrapure water after both steps.

The ionene and polyelectrolytes were deposited onto the negatively charged substrate as described previously.[1,2] After each adsorption step the surface of the film was thoroughly rinsed and then blown dry with a stream of nitrogen gas. First, five bilayers of PAH and CAG were deposited by dipping in the PAH solution (11 unit mM, pH 4.0) and into the CAG solution (5 unit mM, pH 6.3) for 20 min each. Then, 10 bilayers of ionene and CAG were deposited by dipping the substrate alternately into the ionene in DMSO/H_2O (1/1) (0.1 unit mM) and into the CAG solution (5 unit mM, pH 6.3). The quantity of material deposited at each step was deduced from its absorption spectrum, which was determined on a Perkin-Elmer UV/vis spectrophotometer (Lambda 40).

2.4. Measurement of Ellipsometric Thickness. The thickness of the multilayer assemblies of ionene/CAG on a silicon wafer was determined by using an optical ellipsometer (Rudolph/Auto EL). The measurement was preformed using a He/Ne laser 632.8 nm line incident upon the sample at 70°. The ellipsometric parameters, Δ and Ψ, were determined for both the bare clean substrate and the SA film. The so-called DafIBM program supplied by the Rudolph Technologies was employed to determine the thickness values. At least five different sampling points were considered in order to obtain an average thickness value.

2.5. Polarized UV/vis Spectroscopy. The polarized UV/vis spectra were taken with a Perkin-Elmer spectrophotometer (Lambda 40). The orientation of the azobenzene chromophore in ionene/CAG film was estimated from the polarized UV spectra obtained at 45° incidence angle.

2.6. Fourier Transform Infrared Absorption Spectroscopy. The infrared spectra were obtained with Nicolet MAGNA-IR 560 Fourier transform spectrometer with an IR light source and a DTGS KBr detector. The spectra were recorded at an 8 cm^{-1} resolution with 4−16 scans in the 4000−500 cm^{-1} region.

2.7. AFM Imaging. AFM images were obtained in air at room temperature by using a Digital Instruments model Nanoscope IIIa scanning probe microscope. Using a V-shaped and 200 μm long Si_3N_4 cantilever with a nominal spring constant of 0.12 N/m (Nanoprobe, Digital Instruments), topography images were recorded in the conventional height mode (tapping mode, normal AFM) at scan rate of 2−5 Hz.

3. Results and Discussion

3.1. UV/vis Spectrometry Study. Figure 2 compares the spectra of PAZ-6, PAZ-10, and PAZ-12 in DMSO/H_2O (1/1) solution (5 unit mM) with those of the SA multilayer films adsorbed on the fused silica. The maximum absorbance of PAZ-6 was found at 359 nm. That indicates that PAZ-6 exists in solution as a molecularly dispersed state. By extending the spacer chain lengths from 6 to 10 and 12 carbons, the maximum absorbance was blue-shifted to 343 nm in PAZ-10 and drastically about 50 nm to 309 nm in the case of PAZ-12, respectively. According to the spectra, PAZ-10

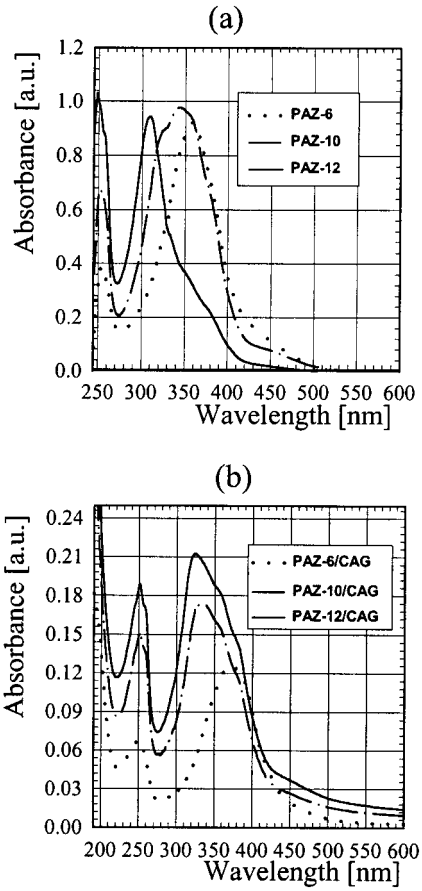

Figure 2. UV/vis spectra of PAZ-6, PAZ-10, and PAZ-12 in 5 unit mM DMSO/H_2O (1/1) solution (A) and in multilayer assemblies (B).

and PAZ-12 form H-aggregates that were generated by an excitonic interaction of the *trans*-azobenzenes arranged "face-to-face" in dimers or higher aggregates. It should be here noted that the extension of the spacer chain length from 10 to 12 carbons caused the drastic change of the aggregate state of azobenzene. In addition, the narrow bandwidth of PAZ-12 is indicated to the formation of the uniform aggregates in comparison with the broad band of PAZ-10. Although it was reported that the chain length of the amphiphile influences the aggregate state of azobenzene,[30] we describe for the first time that the variation of spacer chain length of azobenzene ionenes can also affect the aggregate states of the chromophores.

The maximum absorbance of azobenzene ionenes in the multilayer assemblies was shifted from 359 to 371 nm with the formation of J-aggregates for PAZ-6, while the H-aggregate states were changed for PAZ-10 and PAZ-12 with the spectral shifts from 343 to 333 nm and from 309 to 323 nm, respectively. That might be due to the changed aggregate state of azobenzene that takes place from the realignment of the ionene spacer chains in the multilayer assemblies on a solid substrate.

The dependence of the maximum absorbance of the azobenzene ionenes in multilayer assemblies on the spacer chain length is summarized in Table 2 in comparison with that in solution.

Figure 3 shows the maximum $\pi\pi^*$ absorbance of azobenzene ionenes at 371 (PAZ-6), 333 (PAZ-10), and 323 nm (PAZ-12) as a function of the number of bilayers deposited. The deposition process was repeated 10 times in this experiment in order to confirm that the adsorp-

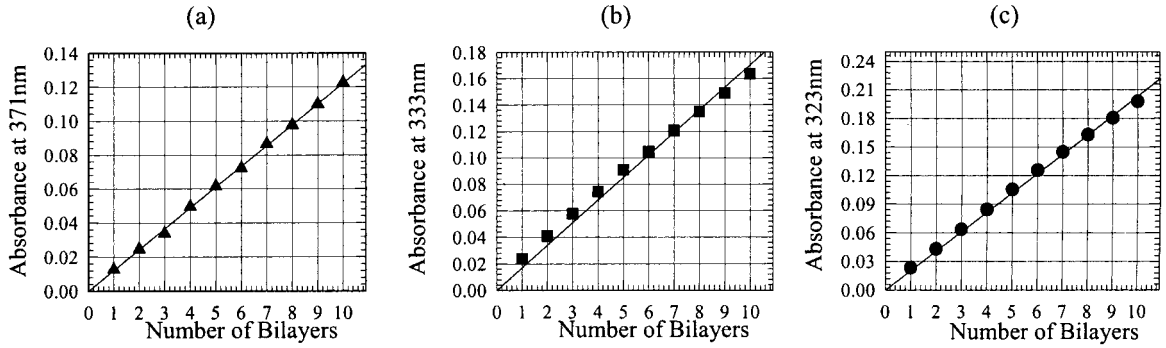

Figure 3. Plot of the absorbance vs the number of deposition cycles for the systems: (a) PAZ-6/CAG, (b) PAZ-10/CAG, and (c) PAZ-12/CAG.

Table 2. UV/vis Spectroscopic Study on the Aggregate State of PAZ-6, PAZ-10, and PAZ-12 in Solution and in Multilayer Assemblies

ionenes	abs max (nm) in DMSO/H_2O (1/1)	abs max (nm) in SA multilayers with CAG	spectral shift, $\Delta\lambda$ (nm)	types of aggregates
PAZ-6	359	371	−12	J
PAZ-10	343	333	+10	H
PAZ-12	309	323	−14	H

tion occurs essentially uniformly, the same amount being deposited on each cycle. A linear fit of data yields an average increase of the optical density of 0.0122 (R = 0.9997) for PAZ-6, 0.0170 (R = 0.9981) for PAZ-10, and 0.0204 (R = 0.9994) for PAZ-12 per layer of azobenzene ionene. The change of the optical density per bilayer reflects the amount of the ionenes adsorbed. Interestingly, it should be noted here that the quantity of polyions adsorbed increased markedly with spacer chain length. As seen in the UV spectra of ionene solution, increasing the spacer chain length affects the formation of the aggregate states in solution that seem to cause the increased adsorption of ionenes on the oppositely charged surface. Again, it is seen that the ionene with longer spacer chain forms more densely packed monolayers.

3.2. Tilt Angle Measurement of Chromophores. Through the linear dichroism measurements, one can obtain the main values of the polarizability tensors which are related to the characteristic angles defining molecular orientation. On this basis, tilt angle of the azobenzene chromophore in the alternating multilayer of ionenes and CAG was estimated from the UV−vis linear dichroism spectra, referring to an optoelectric equation reported by Vandevyver et al.[31] In these processes, the infinite dilution hypothesis was applied, and the $\pi\pi^*$ transition dipole was assumed to be directed along the molecular axis of azobenzene. On the basis of the refractive indices of the fused silica and ionenes (1.47 and 1.43),[31] the average tilt angle of the azobenzene chromophores with respect to the substrate normal was calculated to be 34.9°, 39.4°, and 46.3° for PAZ-6/CAG, PAZ-10/CAG, and PAZ-12/CAG multilayers, respectively. Clearly, it has been shown that the azobenzenes adopt a more tilted alignment in the direction to the surface with increasing the spacer chain length. From a molecular modeling calculation (CPK model), the molecular length of the repeat unit of the ionenes, in fully stretched form, is estimated to be 32.8, 42.4, and 47.4 Å for PAZ-6, PAZ-10, and PAZ-12, respectively. According to the simple model reconstructed based on the tilt angle measurement and theoretical molecular length of repeat unit, the thickness of the ionene monolayer was calculated to be 17.8, 26.1, and 32.3 Å for PAZ-6, PAZ-10, and PAZ-12, respectively. On the other hand, according to the semiempirical quantum mechanical calculation, the alkyl chains in the ionenes are presumed to be tilted by ca. 7° from the azobenzene moiety. On these grounds, consulting the UV−vis linear dichroism spectra and the theoretical molecular lengths of the repeating units, the theoretical thickness of the ionene monolayers is predicted to be 2.55−2.84, 3.02−3.49, and 2.94−3.57 nm for PAZ-6, PAZ-10, and PAZ-12, respectively. These theoretical thickness values are listed in the fourth column of Table 3.

3.3. Ellipsometric Thickness of Multilayer Assemblies. Figure 4 shows the plot of the thickness vs the number of bilayer of ionenes and CAG. The thickness of bilayers increased uniformly with the adsorption cycles. From the slopes in Figure 4, we can predict the thickness per bilayer of PAZ-6/CAG, PAZ-10/CAG, and PAZ-12/CAG to be 2.63, 3.31, and 3.82 nm per bilayer, respectively. Since the true refractive indices are unknown, we assumed the film refractive index to be 1.54 in analyzing the ellipsometric data. The thickness of ionene monolayer can be calculated to be 2.02, 2.74, and 3.22 nm for PAZ-6, PAZ-10, and PAZ-12, respectively, assuming the thickness of a CAG layer to be 0.64 nm, which was estimated from the determined total thickness of the five bilayers of PAH/CAG. The ellipsometric thickness values of the ionene monolayers thus obtained are also listed in the third column of Table 3.

It may be intriguing that the ellipsometric thicknesses of the ionene monolayers are much smaller than those calculated from the model, especially in the case of PAZ-6/CAG and PAZ-10/CAG multilayer assemblies. Nonetheless, it has to be borne in mind that the thickness determined by ellipsometry is the spatially averaged values and thus does not reflect the real molecular height. The smaller ellipsometric thicknesses of the ionene monolayers for PAZ-6 and PAZ-10 seem thus to be attributed to the fact that ionenes with shorter spacer chain length are to form rather sparely packed monolayers on the solid substrate. However, as concluded from the analysis of the UV/vis spectra of PAZ-12, ionenes with longer spacer chain length form very densely packed monolayers; thereby, the ellipsometric thickness of PAZ-12 becomes in good agreement with that estimated from a model calculation.

3.4. FTIR Spectroscopy. It has been well-estimated that the C−H stretching region (2800−3000 cm^{-1}) provides information on the orientation of the methylene chains in two-dimensional self-assembled monolayers (2D-SAMs). That is, the peak positions of the symmetric

Table 3. Average Thickness of Bilayers and Ionene Monolayers

charged adsorbed pairs	thickness of bilayers [nm]	thckness of ionene monolayers from ellipsometry[a] [nm]	thickness of ionene monolayers from model calculation[b] [nm]	thickness of ionene monolayers from AFM[c] [nm]
PAZ-6/CAG	2.66 ± 0.02	2.02	2.55−2.84	2.71
PAZ-10/CAG	3.38 ± 0.11	2.74	3.02−3.49	
PAZ-12/CAG	3.86 ± 0.09	3.22	2.94−3.57	3.78

[a] The average thickness of a bilayer of PAH/CAG was determined to be 1.27 ± 0.07 nm by ellipsometry. The thickness of a CAG monolayer was assumed to be 0.64 nm for estimating the thickness of an ionene monolayers. [b] Estimated by referring to the theoretical molecular length of the repeat unit of the ionenes (CPK model), the tilt angle of the chromophore with respect to the substrate normal determined by polarized UV/vis spectrometry, and the tilt angle of the alkyl chains from the azobenzene estimated from an semiempirical quantum mechanical calculation. See text. [c] See section 3.5.

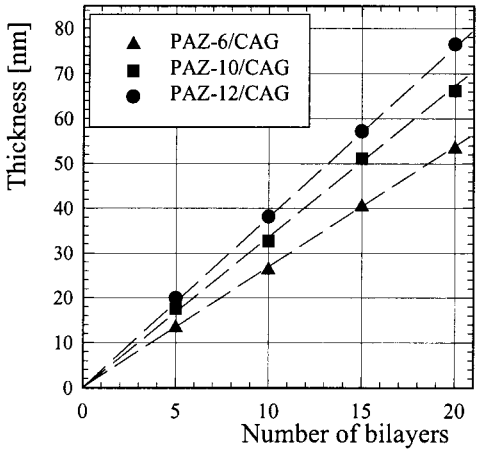

Figure 4. Ellipsometric thickness vs number of bilayers of PAZ-6/CAG (▲), PAZ-10/CAG (■), and PAZ-12/CAG (●) on a silicon substrate.

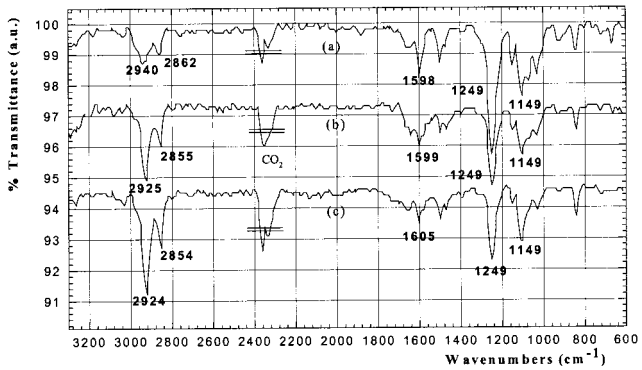

Figure 5. FTIR transmittance spectra of the self-assembled films composed of 10 bilayers of PAZ-6/CAG, PAZ-10/CAG, and PAZ-12/CAG on silicon wafer pretreated with five bilayers of PAH/CAG. (The contribution of the PAH/CAG layers has been subtracted in each spectra shown.)

(ν_s) and antisymmetric (ν_{as}) CH_2 stretching vibration are a very invaluable indicator of the ordering of the alkyl chains.[32,33] In crystalline polyethylene,[34] ν_{as} lies at 2920 cm^{-1} and ν_s is found at 2850 cm^{-1}, while they appear around 2928 and 2856 cm^{-1}, respectively, in solution state; the higher energies for the methylene stretching vibrations of polyethylene in solution are thought to arise from a greater population of gauche defects. On these grounds, invoking the fact that the ν_s and ν_{as} values appear at 2920 and 2850 cm^{-1}, respectively, for hexadecanethiolate monolayers on a gold surface, Nuzzo et al.[33a,c] concluded that the number of gauche defects in the methylene chains was negligibly small. Similarly, Porter et al.[33c] also analyzed the reflection−absorption infrared (RAIR) spectra of a wide range of 2D alkanethiolate monolayers on a gold surface by comparing their ν_s and ν_{as} values with those of crystalline hexadecanethiol (2918, 2851 cm^{-1}) and liquid heptanethiol (2924, 2855 cm^{-1}). They found that monolayers with chains longer than hexanethiol were highly ordered, whereas the smaller molecules most resembled the liquid state, presumably with a higher density of gauche defects. To obtain the information about the conformation of the alkyl chains, we have thus attempted to analyze the transmission FTIR spectra of the multilayer assemblies as shown in Figure 5.

As can be seen in Figure 5, the symmetric and asymmetric stretching bands of the methylene groups are observed respectively at 2855 and 2925 cm^{-1} for the PAZ-10 and at 2854 and 2924 cm^{-1} for PAZ-12 multilayer assemblies, while they appear at 2941 and 2862 cm^{-1} for PAZ-6 multilayers. To obtain the structural information on the alkyl chains of the ionenes, one has to consider that the actually observed ν_{as} and ν_s peaks in Figure 5 are strongly contributed by the anionic polyelectrolyte; the alkyl chains of CAG must take a disordered conformation. In any event, the peak positions observed for the PAZ-6 multilayers clearly indicate that the alkyl chains are strongly disordered. On the other hand, the peak positions observed for the PAZ-10 and PAZ-12 are to assume more or less ordered conformation on the solid substrates; the deviation of the peak positions from those of the reported crystalline alkyl chains is attributed to CAG. That is, the ionene with a chain of six carbons is presumed to be present as a liquid state with a higher density of gauche defects, while that with a chain with more than 10 carbons is present as a crystalline-like state between the layers of anionic polyelectrolytes.

3.5. AFM Images. To obtain the information on the dependence of the space chain length on the domain structure and the surface roughness of the azobenzene ionenes, we have recorded the AFM images for the PAZ-6 and PAZ-12 2D-SAMs on mica, shown in Figure 6, A and B, respectively. The AFM image recorded in the tapping mode is given in a top view presentation with the lighter areas denoting higher regions and the darker areas representing lower regions. As can be seen in Figure 6A, the SAM of PAZ-6 on a mica exhibits a granular structure with the uniform size ranging in a region of 2−4 nm. The SAM of PAZ-12 on a mica shows also the similar domain structures, but the size of the granules is much larger than that of PAZ-6, as concluded from the analysis of the UV/vis absorbance spectroscopy. From the section analyses, the thicknesses of the PAZ-6 and PAZ-12 monolayers are determined to be 2.71 and 3.78 nm, respectively. These values are also listed in Table 3. As can be seen in Table 3, the thickness values obtained from the AFM analyses are in fact surprisingly consistent with those from the theoretical model calculations. This supports our previous arguments that the thickness determined by ellip-

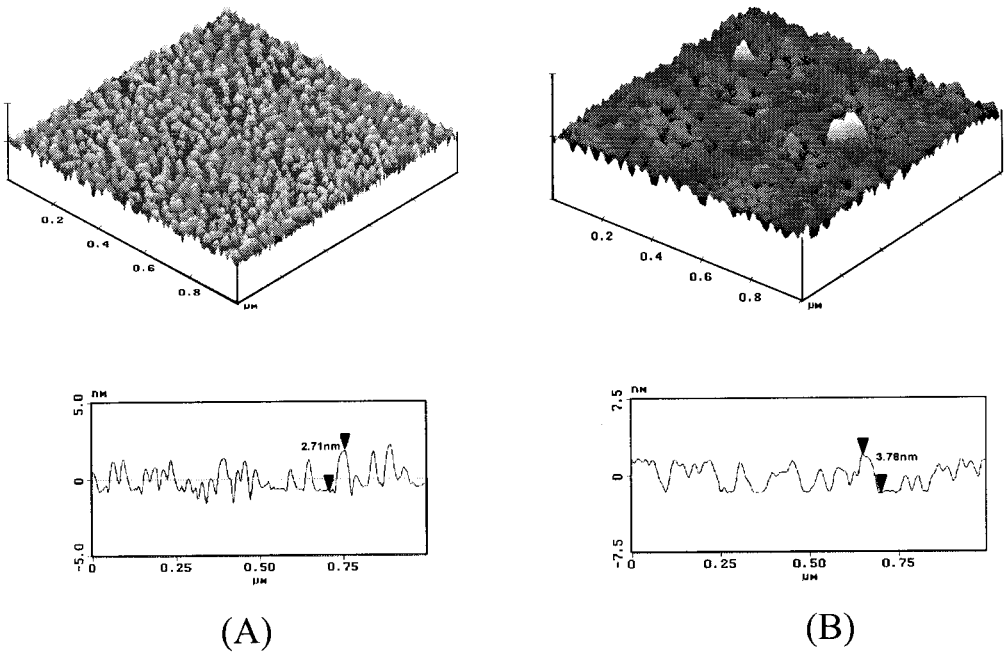

Figure 6. Tapping mode AFM image (1.0 μm × 1.0 μm) of the SAMs on mica: (A) PAZ-6; (B) PAZ-12. Upper parts show raw AFM images, and lower ones represent the relative height profiles against the lowest point of the whole two-dimensional image.

sometry is the spatially averaged values and thus does not reflect the real molecular height.

4. Summary and Conclusions

Azobenzene ionenes with spacer chain length in the range 6−12 are adsorbed as uniform layers onto a surface of opposite charge, and this leads to the formation of alternating multilayer assemblies. The structure of the multilayer assemblies was studied with various characterization techniques, such as polarized UV/vis and FTIR spectroscopy, ellipsometry, and atomic force microscope (AFM).

The UV/vis absorption spectrum of the azobenzene ionenes in DMSO/H_2O (1/1) shows that PAZ-6 exists in a molecularly dispersed state, while PAZ-10 and PAZ-12 formed H-aggregates. This indicates that the spacer chain strongly affects the "face-to-face" packing of the chromophores. In line with the UV/vis absorbance data, the FTIR spectra showed that the frequencies of the ν_{as} and ν_s modes of the methylene groups are significantly lowered by extending the spacer chain lengths, revealing that the alkyl chains become ordered upon the increase in the chain lengths. Although the thickness values of the ionene monolayers determined from ellipsometry were somewhat smaller than those predicted from a model calculation, the height of the monolayer obtained from the section analyses of the AFM images was surprisingly consistent with the model calculation.

Although the UV−vis, infrared, and ellipsometry results strongly suggested that the multilayer buildup proceeded homogeneously and regularly with the formation of the internal ordering in layers, we have also to mention that the Bragg peaks were barely identified in the X-ray reflectivity measurements, however (data not shown). The lack of the Bragg peaks indicates that all charged groups are not perfectly aligned close to the two interfaces of a single layer due to large overlaps between adjacent layers in this multilayer systems. At the moment, the extent of interpenetration of the PAZ polyionenes into the anionic polyelectrolyte layers is indeterminate due to the absence of information on the morphology of the anionic CAG layers. In conjunction with this, we plan to incorporate an inorganic layer to achieve a discrete layering of the polymers. Nonetheless, this work clearly dictates that the electrostatic deposition technique can lead to internally ordered multilayers if one of the oppositely charged polyelectrolytes employed has a tendency to form lamellae, and we have demonstrated an example of a polyelectrolyte with such a lamellar habit. Finally, we believe that the resulting control of molecular order in multilayer assembly will enhance the usefulness of the electrostatic layer-by-layer adsorption method as a thin film technology.

Acknowledgment. This paper was supported by Korea Science and Engineering Fund (Contact 98-0702-04-01-3) and partially by NON DIRECTED RESEARCH FUND, Korea Research Foundation. Kim Kwan also acknowledge the Korea Science and Engineering Foundation for providing the instrument maintenance fund through the Center for Molecular Catalysis at Seoul National University.

References and Notes

(1) Decher, G.; Hong, J.-D. *Makromol. Chem. Macromol. Symp.* **1991**, *46*, 321.
(2) Decher, G.; Hong, J.-D.; Schmitt, J. *Thin Solid Films* **1992**, *210/211*, 831.
(3) Lvov, Y.; Decher, G.; Sukhorukov, G. *Macromolecules* **1993**, *26*, 5396.
(4) Donth, E.; Walther, D.; Shilov, V. N.; Knippel, E.; Budde, A.; Lowack, K.; Helm, C. A.; Möhwald, H. *Langmuir* **1997**, *13*, 5294.
(5) Hong, J.-D.; Lowack, K.; Schmitt, J.; Decher, G. *Prog. Colloid Polym. Sci.* **1993**, *93*, 98. Lvov, Y.; Ariga, K.; Ichinose, I.; Kunitake, T. *J. Am. Chem. Soc.* **1995**, *117*, 6117.
(6) Kleinfeld, E. R.; Ferguson, G. S. *Science* **1994**, *265*, 370.
(7) Keller, S. W.; Kim, H. N.; Mollouk, T. E. *J. Am. Chem. Soc.* **1994**, *116*, 8817.
(8) Lvov, Y.; Ariga, Ichinose, K. I.; Kunitake, T. *Langmuir* **1996**, *12*, 3038.
(9) Kotov, N. A.; Dékány, I.; Fendler, J. H. *J. Phys. Chem.* **1995**, *99*, 13065.
(10) Feldheim, D. L.; Crabar, K. C.; Natan, M. J.; Mallouk, T. E. *J. Am. Chem. Soc.* **1996**, *118*, 7640.

(11) Schmitt, J.; Decher, G.; Dressik, W. J.; Branduo, S. L.; Geer, R. E.; Shashidhal, R.; Calvert, J. M. *Adv. Mater.* **1997**, *9*, 61.
(12) Freeman, R. G.; Grabar, K. C.; Allison, K. J.; Bright, R. M.; Davis, J. A.; Guthrie, A. P.; Hommer, M. B.; Jackson, M. A.; Smith, P. C.; Walter, D. G.; Natan, M. J. *Science* **1995**, *267*, 1629.
(13) Cooper, T.; Campbell, A.; Crane, R. *Langmuir* **1995**, *11*, 2713.
(14) Yoo, D.; Lee, J.-K.; Rubner, M. F. *Mater. Res. Soc. Symp. Proc.* **1996**, *413*, 395.
(15) Zhang, X.; Gao, M.; Kong, X.; Sun, Y.; Shen, J. *J. Chem. Soc., Chem. Commun.* **1994**, 1005.
(16) Araki, K.; Wagner, M. J.; Wrighton, M. S. *Langmuir* **1996**, *12*, 5393.
(17) Sellergren, B.; Swietlov, A.; Amebrant, T.; Unger, K. *Anal. Chem.* **1996**, *68*, 402. Mao, G.; Tsao, Y.; Tirrell, M.; Davis, H. T. *Langmuir* **1993**, *9*, 3461. Saremi, F.; Tieke, B. *Adv. Mater.* **1995**, *7*, 378. Saremi, F.; Maassen, E.; Tieke, B. *Langmuir* **1995**, *11*, 1068. Saremi, F.; Lange, G.; Tieke, B. *Adv. Mater.* **1996**, *8*, 923.
(18) Ariga, K.; Lvov, Y.; Kunitake, T. *J. Am. Chem. Soc.* **1997**, *119*, 2224.
(19) Cheung, J. H.; Fou, A. F.; Rubner, M. F. *Thin Solid Films* **1994**, *244*, 958. Fou, C.; Onitsuka, O.; Ferreira, M.; Rubner, M. F. *J. Appl. Phys.* **1996**, *79*, 7501.
(20) Hong, J.-D.; Kim, D. S.; Char, K. H.; Jin, J. I. *Synth. Met.* **1997**, *84*, 815.
(21) Kim, H. N.; Keller, S. W.; Mallouk, T. E. *Chem. Mater.* **1977**, *9*, 1414.
(22) Cochin, D.; Passmann, M.; Wilbert, G.; Zentel, R.; Wischerhoff, E.; Laschewsky, A. *Macromolecules* **1977**, *30*, 4775.
(23) Mao, G.; Tsao, Y.; Tirrell, M.; Davis, H. T.; Hessel, V.; Ringsdorf, H. *Langumir* **1995**, *11*, 942.
(24) Hong, J.-D.; Park, E. S.; Park, A. L. LB8 Conference, Asilomar, 1997.
(25) Saremi, F.; Tieke, B. *Adv. Mater.* **1998**, *10*, 388.
(26) Hong, J.-D.; Park, E. S.; Park, A. L. *Bull. Korean Chem. Soc.* **1998**, *19*, 1156.
(27) Hong, J.-D.; Park, E. S.; Park, A. L. *Langmuir* **1999**, *15*, 6515.
(28) Kunitake, T.; Tsuge, A.; Takarabe, K. *Polym. J.* **1985**, *17*, 633.
(29) Reck, B. Diploma, Mainz, 1985.
(30) Kunitake, T. *Modern Trends of Colloid Science in Chemistry and Biology*; Birkhäuser Verlag: Basel, 1985; p 34.
(31) Vandevyver, M.; Barraud, A.; Teixier, R.; Maillard, P.; Gianotti, C. *J. Colloid Interface Sci.* **1982**, *85*, 571.
(32) (a) Dubois, L. H.; Nuzzo, R. G. *Annu. Rev. Phys. Chem.* **1992**, *43*, 437. (b) Ulman, A. *An Introduction to Ultrathin Organic Films*; Academic: New York, 1991. (c) Bain, C. D.; Whitesides, G. M. *Angew. Chem., Int. Ed. Engl.* **1989**, *28*, 506.
(33) (a) Nuzzo, R. G.; Fusco, F. A.; Allara, D. L. *J. Am. Chem. Soc.* **1987**, *109*, 2358. (b) Nuzzo, R. G.; Dubois, L. H.; Allara, D. L. *J. Am. Chem. Soc.* **1990**, *112*, 558. (c) Porter, M. D.; Allara, D. L.; Chidsey, C. E. D. *J. Am. Chem. Soc.* **1987**, *109*, 3559.
(34) (a) Snyder, R. G.; Straus, H. L.; Elliger, C. A. *J. Phys. Chem.* **1982**, *86*, 5145. (b) Snyder, R. G.; Maronelli, M.; Strauss, H. L.; Hallmark, V. M. *J. Phys. Chem.* **1986**, *90*, 5623.

MA000293G